Damping analysis of Floating Offshore Wind Turbine (FOWT): a new control strategy reducing the platform vibrations

Matteo Capaldo[1] and Paul Mella[2]

[1]TotalEnergies OneTech, Palaiseau, France
[1,2]Ecole Polytechnique, Institut Polytechnique de Paris, Palaiseau, France

Correspondence: Matteo Capaldo (matteo.capaldo@totalenergies.com)

Abstract. In this paper, the coupled dynamics of the floating platform and the wind turbine rotor is analysed. In particular, the damping is explicitly derived from the coupled equations of rotor and floating platform. The analysis of the damping leads to the study of the instability phenomena obtaining the explicit conditions that lead to the Non Minimum Phase Zero (NMPZ). Two NMPZs are analysed, one related to the rotor dynamics and the other one to the platform pitch dynamics. The latter is a novelty and an explicit condition is introduced in this work for its verification. In the second part of the paper, from the analysis of the damping of the floating platform, a new strategy for the control of Floating Offshore Wind Turbines (FOWTs) is proposed. This strategy allows one to impose to the controller an explicit level of damping in the platform pitch motion without changing the period of platform pitching. Finally the new strategy is compared to the one without compensation by performing aero-hydro-servo-elastic numerical simulations of a reference FOWT. Generated power, movements, blade pitch and tower base fatigue are compared showing that the new control strategy can reduce fatigue in the structure without affecting the power production.

1 Introduction

Wind energy is an important source of renewable energy and it has a very high potential in both onshore and offshore. In terms of installed capacity, onshore wind is still the largest contribution. However, in the next years, the new annual offshore installed capacity is estimated to exceed 30 GW by 2030, in order to stay on-track for a netzero/$1.5°\,C$ pathway (Lee et al., 2022). In offshore, there is a growing interest in floating foundations. In fact, FOWTs would allow access to good wind resource locations that are not suitable for fixed-bottom foundations.

In that context, the levelized cost of energy (LCOE) of offshore wind farms needs to be decreased to be competitive with respect to onshore wind. This is especially true for the FOWTs. One effective way to achieve this objective is to investigate different strategies for the control of the FOWTs in order to improve it with respect to the LCOE. As explained in (Bianchi et al., 2007), the minimisation of the LCOE involves a series of partial objectives, energy capture, mechanical loads and power quality. These objectives are actually closely related and sometimes conflicting and they should not be pursued separately. Hence, the question is to find a well balanced compromise among them. Considering FOWTs, this optimization problem increases in complexity since the movements of the floating platform interact with the feedback control loop. Moreover, the

25 coupling between the platform movements, the rotor dynamics and the blade pitch control can lead to oscillating (or not damped) stability or even to unstable conditions (Larsen et al., 2007).

The nature and the set of control parameters leading to the instability can variate from one platform design to another one, e.g., barge, spare, semi-sub or tension-leg platform. However, for each of the platforms, there are sets of design and control parameters leading to oscillating stability or instability (Fleming et al., 2014). The issue come from the fact that in above rated

30 wind speed, the blade pitch regulates the speed by increasing the angle of attack to feather. For a FOWT, when the platform has a forward motion, the rotor experiences an increasing wind speed. Consequently, the blade pitch control increases the angle of attack to feather and, hence, reduces the aerodynamic torque and regulates the rotor speed. However, it also reduces the rotor thrust that induces a further forward motion. So the blade pitch control amplifies the original forward motion of the platform because the floating platform surge and pitch natural frequencies are in the bandwidth of the blade pitch control.

35 Solutions exist to avoid this phenomenon. The first one and the most common in literature is to reduce the blade pitch control proportional and integral gains in order to reduce its bandwidth and exclude the platform pitch and surge natural frequencies (Jonkman et al., 2008; Larsen et al., 2007). However, this solution do not completely solve the problem and, moreover, the price to pay is to have a less reactive blade pitch control that allows important over-speeds of the rotor. Alternative methods use additional sensing, such as nacelle fore-aft acceleration measurements or platform gyroscopes, to improve the performance of

40 the pitch controller. In (Lackner et al., 2009) and (Lenfest et al., 2020), the platform pitch velocity is used to adjust the rated speed set-point to reduce platform motions. However, the platform pitch damping analysis is not investigated and the link with the compensation parameter is not given. Higher order controllers, such as a linear quadratic regulator (LQR) are applied and evaluated in (Ma et al., 2018). Disturbance accommodating controller (DAC) is evaluated in (Menezes et al., 2018) and it is coupled with individual pitch control (IPC) in (Namik et al., 2011). A nonlinear pitch and torque controller using wind preview

45 is designed in (Sarkar et al., 2020) and (Schlipf et al., 2013), giving promising results.

The control strategy proposed in this work shares some similarities to the one introduced in (Lackner et al., 2009) and (Lenfest et al., 2020). As introduced in this paper, in fact, the rated generator speed is no longer a constant value but a function of the platform pitch velocity and the blade pitch is used to damp the floating platform pitch. However, differently from (Lackner et al., 2009), the ratio between proportional and integral gains of the correction can be considered different for the

50 platform pitch motion and the rotor speed. This choice, in fact, can be not optimal for some cases. Differently from (Lenfest et al., 2020), a mathematical frame is given to define the compensation to the platform pitch and the explicit analytical form of it is given. Moreover, a second compensation is considered in the control strategy proposed in this work. It is to solve the Non Minimum Phase Zero (NMPZ) effects caused by the blade pitch on the rotor rotational dynamics. It is already introduced in (Stockhouse et al., 2021) and it is, in this work, analytically developed. The study of the NMPZs brings to a new NMPZ

55 phenomenon, described for the first time in this work. This is the NMPZ caused by the blade pitch on the platform dynamics. This new phenomenon is analytically developed leading to the explicit condition to verify it. However, the compensations proposed by this model can't correct it.

The novelty of this work is related to the FOWT damping analysis, i.e., the damping obtained by coupling the rotor and the platform pitch dynamics. This damping is explicitly derived from the coupled equations of rotor and floating platform. This

analysis leads to the study of the instability phenomena underlining the conditions leading to the NMPZ. One new NMPZ, never discussed in literature, is discovered and analysed in this work. The domain of the instability of the platform is explicitly derived from the coupled system of equations. The control strategy proposed relies on this analysis and it allows to impose an explicit level of damping in the platform pitch motion to the controller without changing the period of platform pitching. This explicit form of the damping in the platform pitch dynamics is a novelty of this work.

The chosen strategy is, then, compared to the one which does not consider a platform pitch compensation. The latter neglects the following phenomenon: the blade feather reduces the aerodynamic thrust and, thus, a part of the opposing force on the platform is neglected.

The document is organized as follows. In Section 2, the equations of the FOWT system are described with the considered degrees of freedom and their coupling terms. Section 2.1 presents the control model considered in this work. The closed loop feedback system is then analysed in Section 2.3, leading to the definition of the conditions for the NMPZs. For this controller, a new control strategy dedicated to FOWTs, named ζ_{plt}-fixed is presented and analytically derived in Section 2.4 and 2.5. Some numerical tests are presented and commented in Section 3.

2 Floating Offshore Wind Turbine and its controller

The floating offshore wind turbine (FOWT) is represented by a system of two degrees of freedom, namely the rotor speed Ω and the platform pitch angle, Φ. Surge degree of freedom is not considered in this model. In fact, surge speed of the FOWT can be neglected with respect to the speed at nacelle generated by the pitch motion of the platform. This is already mentioned in (Sarkar et al., 2020b), where the authors remarked that the dynamics of the surge motion is much slower than the one of the pitch. Hence, the surge can be considered as a static offset in the position of the wind turbine without any effects on the controller.

Two control parameters, B (blade pitch) and τ_g (generator torque), and two external disturbances, V (wind speed) and W (waves speed) are considered. For all the values that form a given operating point (namely $\Omega, \Phi, B, T_g, V, W$), the notation $X = \bar{x} + x$ is adopted, with x being the small perturbation of a steady-state operating point $\bar{x}$.

The model is, then, based on the two fundamental equations:

$$\dot{\Omega}_g = \frac{N_g}{J_r}(T_a - N_g T_g) \tag{1}$$

$$J_t \ddot{\Phi} + D_t \dot{\Phi} + K_t \Phi = h_t F_a + \tau_w \tag{2}$$

where Ω_g is the generator speed, hereafter noted Ω, T_a and T_g are the aerodynamic and electric torque, N_g is the gearbox ratio and J_r is the rotor inertia. J_t is the total system moment of inertia about the pitch rotation, D_t is the natural damping coefficient (assumed constant), K_t is a spring-like restoring coefficient (mainly given by the mooring lines of the floating platform), h_t is the height of the rotor (approximately the tower length), F_a is the aerodynamic force flowing from the rotor to the system and τ_w is the overturning moment given by the waves.

Once a steady-state operating point $\bar{x}$ is reached, the same two equations can be applied to any small variations x around this operating point. Equations 1 and 2 applied on X can be written:

$$\dot{\omega} = \frac{N_g}{J_r}(\tau_a - N_g \tau_g) \tag{3}$$

95 $\quad J_t \ddot{\phi} + D_t \dot{\phi} + K_t \phi = h_t dF_a + d\tau_w \tag{4}$

The infinitesimal thrust and torques satisfy $T_g = \bar{\tau}_g + \tau_g$, $T_a = \bar{\tau}_a + \tau_a$, $F_a = \bar{F}_a + dF_a$ and $\tau_w = \bar{\tau}_w + d\tau_w$. By considering small perturbations of a steady-state operating point (given by $\Omega, \Phi, B, T_g, V, W$), it allows one to use the following linear forms:

$$\tau_a = \frac{\partial \tau_a}{\partial \omega}\omega + \frac{\partial \tau_a}{\partial v}v_r + \frac{\partial \tau_a}{\partial \beta}\beta \tag{5}$$

100 $\quad dF_a = \dfrac{\partial F_a}{\partial \omega}\omega + \dfrac{\partial F_a}{\partial v}v_r + \dfrac{\partial F_a}{\partial \beta}\beta \tag{6}$

$$d\tau_w = \frac{\partial \tau_w}{\partial w}w \tag{7}$$

Note that F_a and τ_w are separated for clarity, which explains why dF_a does not depend on a w perturbation. Moreover, the hypothesis of ϕ being small allows one to remove the terms $\frac{\partial \tau_a}{\partial \phi}\phi$, $\frac{\partial F_a}{\partial \phi}\phi$ and $\frac{\partial \tau_w}{\partial \phi}\phi$.

Relative wind v_r is the wind velocity in rotor reference frame, it is computed from v by:

105 $\quad v_r = v - h_t \dot{\phi} \tag{8}$

Under the assumption of ϕ being small, $h_t \dot{\phi}$ represents the rotor fore-aft velocity in a fixed global reference frame.

Equations 1 and 2 applied to small perturbations of a steady-state point can therefore be expressed in the linear form:

$$\dot{\omega} = \frac{N_g}{J_r}\left(\frac{\partial \tau_a}{\partial \omega}\omega + \frac{\partial \tau_a}{\partial v}(v - h_t \dot{\phi}) + \frac{\partial \tau_a}{\partial \beta}\beta - N_g \tau_g\right) \tag{1'}$$

110 $\quad J_t \ddot{\phi} + D_t \dot{\phi} + K_t \phi = h_t\left(\dfrac{\partial F_a}{\partial \omega}\omega + \dfrac{\partial F_a}{\partial v}(v - h_t \dot{\phi}) + \dfrac{\partial F_a}{\partial \beta}\beta\right) + \dfrac{\partial \tau_w}{\partial w}w \tag{2'}$

Those coupled second order equations yield the following four dimensional state-space model:

$$\dot{x} = A_0 x + B_c u_c + B_d u_d \tag{9}$$

Where $x = (\theta, \dot{\theta}, \phi, \dot{\phi})^T$, $\theta = \int \omega$ (i.e. $\dot{\theta} = \omega$), $u_c = (\beta, \tau_g)^T$ and $u_d = (v, w)^T$, and :

$$A_0 = \begin{bmatrix} 0 & 1 & 0 & 0 \\ 0 & \frac{N_g}{J_r}\frac{\partial \tau_a}{\partial \omega} & 0 & -h_t \frac{N_g}{J_r}\frac{\partial \tau_a}{\partial v} \\ 0 & 0 & 0 & 1 \\ 0 & \frac{h_t}{J_t}\frac{\partial F_a}{\partial \omega} & -\frac{K_t}{J_t} & -\frac{1}{J_t}(D_t + h_t^2 \frac{\partial F_a}{\partial v}) \end{bmatrix} \quad B_c = \begin{bmatrix} 0 & 0 \\ \frac{N_g}{J_r}\frac{\partial \tau_a}{\partial \beta} & -\frac{N_g^2}{J_r} \\ 0 & 0 \\ \frac{h_t}{J_t}\frac{\partial F_a}{\partial \beta} & 0 \end{bmatrix} \quad B_d = \begin{bmatrix} 0 & 0 \\ \frac{N_g}{J_r}\frac{\partial \tau_a}{\partial v} & 0 \\ 0 & 0 \\ \frac{h_t}{J_t}\frac{\partial F_a}{\partial v} & \frac{1}{J_t}\frac{\partial \tau_w}{\partial w} \end{bmatrix} \tag{10}$$

2.1 Control model description

In this section the pitch controller model is described.

The present control model considers ω_r as the reference for ω and 0 as the reference for $\dot{\phi}$. It is based on several SISO (single-input-single-output) feedback loops. It can be seen as a multi-SISO:

– Proportional : $\beta_P = k_P(\Omega - \Omega_r)$

– Integral : $\beta_I = k_I \int (\Omega - \Omega_r) = k_I(\theta - t\Omega_r)$

– Beta platform pitch compensation : $\beta_{comp} = k_\beta(\dot{\Phi}_r - \dot{\Phi})$

– Generator torque platform pitch compensation : $\tau_{g,comp} = k_{\tau_g}(\dot{\Phi}_r - \dot{\Phi})$

Controllers described by the literature considering the same compensations (Abbas et al., 2021; Stockhouse et al., 2021) aim at maintaining ω steady near its rated value by acting on the blade pitch β to variate the aerodynamic torque τ_a with the opposite sign with respect to the rotor relative speed ω. However, this strategy neglects the following phenomenon: the blade feather modifies the aerodynamic thrust F_a. Thus, a part of the opposing force on the platform is neglected. The strategy developed in this paper aims at minimizing ϕ variations with the constraint of maintaining a constant ω. Such a control strategy should reduce the loads on the structures (nacelle, tower and floater). Section 3 considers a full aero-hydro-servo-elastic model to verify this assumption. It is analysed the performance of the control strategy in a FOWT realistic environment reproduced by a numerical twin.

2.2 Global State-Space description

For a FOWT, the objective ot the pitch control is to remain in the equilibrium operating point. It translates in: $\bar{\omega} = \Omega_r$ and $\bar{\dot{\phi}} = \dot{\Phi}_r = 0$. This objective allows one to justify the linear form for of the global equations 1' and 2'. For constant inputs $\bar{v}$ and $\bar{w}$, this operating point is reached by the appropriated pitch ($\bar{\beta}$) and electric torque ($\bar{\tau}_g$).

The control model is, here, introduced into the wind turbine state space description. For small perturbations of this steady-state operating point, the PI controller described previously becomes:

– Proportional:

$$\beta_P = k_P\omega \tag{11}$$

– Integral:

$$\beta_I = k_I \int \omega = k_I\theta \tag{12}$$

– Beta platform pitch compensation:

$$\beta_{comp} = -k_{Beta}\dot{\phi} \tag{13}$$

– Generator torque platform pitch compensation:

$$\tau_{g,comp} = -k_{\tau_g}\dot{\phi} \tag{14}$$

145   Figure 1 shows the entire picture of the control model. This control strategy acts on the two dynamic systems, platform and rotor. Hence, one can appreciate how the bottom-fixed scheme acting on the rotor (ω) with a proportional integral scheme is then corrected by the β_{comp} and the τ_g that depends on the platform pitch dynamics error.

Figure 1. Block diagram of the controller model

The linear expression of $u_c = (\beta, \tau_g)^T$ as a function of $x = (\theta, \dot{\theta}, \phi, \dot{\phi})^T$ is $u_c = K_0 x + u_{c,ol}$ where:

$$K_0 = \begin{bmatrix} k_I & k_P & 0 & -k_\beta \\ 0 & 0 & 0 & -k_{\tau_g} \end{bmatrix} \tag{15}$$

150   is the matrix of the control gains and $u_{c,ol}$ is an optional additional control (open loop) that can be considered. This is useful to analyse the NMPZ in the next section. By replacing it in equation 9, it leads to:

$$\dot{x} = (A_0 + B_c K_0)x + B_c u_{c,ol} + B_d u_d \tag{16}$$

Which leads to define the global matrix of the system of equations:

$$A = (A_0 + B_c K_0) = \begin{bmatrix} 0 & 1 & 0 & 0 \\ k_I \frac{N_g}{J_r} \frac{\partial \tau_a}{\partial \beta} & \frac{N_g}{J_r}(\frac{\partial \tau_a}{\partial \omega} + k_P \frac{\partial \tau_a}{\partial \beta}) & 0 & \frac{N_g}{J_r}(-h_t \frac{\partial \tau_a}{\partial v} - k_\beta \frac{\partial \tau_a}{\partial \beta} + k_{\tau_g} N_g) \\ 0 & 0 & 0 & 1 \\ k_I \frac{h_t}{J_t} \frac{\partial F_a}{\partial \beta} & \frac{h_t}{J_t}(\frac{\partial F_a}{\partial \omega} + k_P \frac{\partial F_a}{\partial \beta}) & -\frac{K_t}{J_t} & \frac{-1}{J_t}(D_t + h_t^2 \frac{\partial F_a}{\partial v} + k_\beta h_t \frac{\partial F_a}{\partial \beta}) \end{bmatrix} \tag{17}$$

155   The time domain system can be rewritten in the complex domain. Using the following notation, $\mathscr{L}\{x(t)\} = \underline{X}$, equation 16 translates into:

$$\underline{X} = (sI - A)^{-1}(B_c \underline{U}_{c,ol} + B_d \underline{U}_d). \tag{18}$$

By defining:

$$B = \begin{bmatrix} B_c & | & B_d \end{bmatrix}, \quad u = \begin{pmatrix} \beta_{ol} \\ \tau_{g,ol} \\ v \\ w \end{pmatrix} \tag{19}$$

160   and

$$G(s) = (sI - A)^{-1}B = \frac{1}{det(sI - A)} Com(sI - A)^T B = \frac{1}{\chi_A(s)} N(s), \tag{20}$$

it leads to:

$$\chi_A(s)\underline{X}(s) = N(s)\underline{U}(s) \tag{21}$$

G(s) is a 4×4 matrix. Every component of which can be written as the quotient of a polynomial in s and $\chi_a(s)$.

165 **2.3   Non minimum phase zeros analysis and resolution (negative damping on the control)**

This section analysis the problem of negative damping by addressing the positions of the zeros of each component of G in the complex plane, i.e. the points where equation 21 is well defined but becomes:

$$\chi_A \, X_0^T \cdot \underline{X} = 0. \tag{22}$$

This translates the fact that s is a NMPZ if it exists a specific X_0^T, such as, for any value of $\underline{U}(s)$, the linear combination
170 $X_0^T N(s)\underline{U}(s)$ gives $X_0^T = 0$.

Physically a X_0^T is equivalent to an infinitesimal shifting along a specific direction of a steady-state point that can not be obtained with any infinitesimal shifting of the input. This phenomenon is better illustrated case by case.

For the rest of the section, an open loop control on β, is considered in order to highlight the NPMZ. Hence, β_{ol} is added to the multiple SISO as already described in 16. Since the feedback control on β can't erase the NMPZ condition, to lighten the
175 formulas, the notation β will be used instead of β_{ol} in this section.

2.3.1 ϕ-NMPZ: negative damping on ϕ control by β

Gain equation in the Laplace domain for $\beta \to \phi$ control is obtained by projecting 21 on the $x = (0, 0, \phi, 0)$ axis and considering only a β perturbation, ie. an input $u = (\beta, 0, 0, 0)$. The resulting equation is:

$$\chi_A(s)\underline{\phi}(s) = N_{3,1}(s)\underline{\beta}(s), \tag{23}$$

180 $$N_{3,1}(s) = \frac{J_r}{N_g}\frac{\partial F_a}{\partial \beta}s^2 + \left(\frac{\partial \tau_a}{\partial \beta}\frac{\partial F_a}{\partial \omega} - \frac{\partial F_a}{\partial \beta}\frac{\partial \tau_a}{\partial \omega}\right)s \tag{24}$$

The condition for the NMPZ on $\beta \to \phi$ control is that $N_{3,1}$ has a root with a real part strictly positive. Assuming that $\beta = \beta_f$, the fine pitch, the previous derivatives are all negative. Hence, the root research of $N_{3,1}$ leads to:

$$\frac{\partial \tau_a}{\partial \omega} \Big/ \frac{\partial \tau_a}{\partial \beta} \quad < \quad \frac{\partial F_a}{\partial \omega} \Big/ \frac{\partial F_a}{\partial \beta} \tag{25}$$

Intuitively, this corresponds to an operating point where τ_a *is rather influenced by* β and F_a *is rather influenced by* ω. This

185 NMPZ does not depend on parameters of the platform, it is only related to WTG performances. However, the amplitude of the phenomenon is related to the platform properties. It is to be noted that this NMPZ has never been highlighted in literature and the control model (with compensations of the platform motions) introduced in Section 2.1 in the feedback control loop does not prevent it. It results only from the characteristic of the FOWT system. Further works should focus on this phenomenon and introduce corrections to prevent it for any FOWT system.

190 In absence of NMPZ, ie. eq. 25 being false, increasing β from a steady-state operating point (ie. setting $d\ddot{\beta} > 0$, $d\dot{\beta} > 0$ and $d\beta > 0$) will always imply a reduction of ϕ. In presence of NMPZ, ie. if eq. 25 is true, the reduction or the increase of ϕ depends on the ratio between $\ddot{\beta}$ and $\dot{\beta}$.

The latter only happens when eq. 25 is verified: increasing blade pitch *reduces τ_a more than it increases F_a* (because τ_a *is rather influenced by* β), thus ω increases and causes F_a to decrease (because F_a *is rather influenced by* ω) and then ϕ to

195 increase. If eq. 25 is not verified, increasing blade pitch β from a steady-state operating point always reduces platform pitch ϕ. In practice, this effect can become an issue for a control algorithm mainly focused on ω stabilization since it generates unexpected platform dynamics. Figure 2 reproduces in the time domain ϕ and ω responses to a β-step input (at $t = 10s$): values (resumed in Table 1) are chosen so that eq. 25 is false: ϕ decreases. On the right, values are chosen so that the eq. 25 is true: ϕ increases even though β has step up.

Table 1. Set of parameters to show the NMPZ of eq. 25

	eq. 25 false	eq. 25 true
$\frac{\partial \tau_a}{\partial v}$	$2980.9\ kN.s$	$3079\ kN.s$
$\frac{\partial F_a}{\partial v}$	$354.8\ kN.s.m^{-1}$	$355.6\ kN.s.m^{-1}$
$\frac{\partial \tau_a}{\partial \omega}$	$-58597.1\ kN.m.s.rad^{-1}$	$-55499.5\ kN.m.s.rad^{-1}$
$\frac{\partial F_a}{\partial \omega}$	$-5658.0\ kN.s.rad^{-1}$	$-5820.4\ kN.s.rad^{-1}$
$\frac{\partial \tau_a}{\partial \beta}$	$-152347.8\ kN.m.rad$	$-160140.5\ kN.m.rad$
$\frac{\partial F_a}{\partial \beta}$	$-16052.2\ kN.rad$	$-15260\ kN.rad$
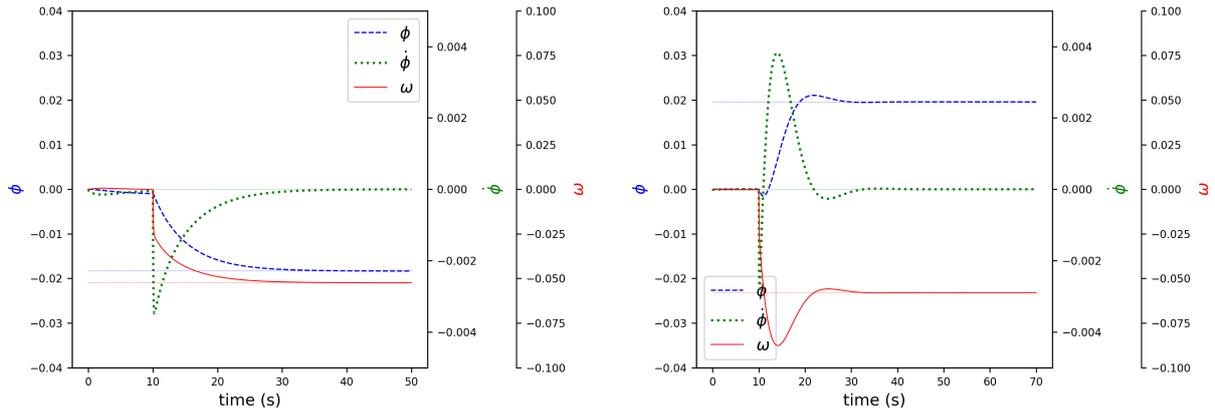
Figure 2. ϕ and ω responses to a β-step input (at $t = 10s$): on the left, values (Table 1) are chosen so that eq. 25 is false: ϕ decreases. On the right, values (Table 1) are chosen so that the eq. 25 is true: ϕ increases even though β has step up.

2.3.2 ω-NMPZ: negative damping on ω control by β

Gain equation in the Laplace domain for $\beta \to \omega$ control is given by:

$$\chi_A(s)\,\underline{\omega}(s) = N_{2,1}(s)\,\underline{\beta}(s) \tag{26}$$

$$N_{2,1}(s) = \frac{J_t}{h_t}\frac{\partial \tau_a}{\partial \beta}s^3 + \left[\frac{D_t}{h_t}\frac{\partial \tau_a}{\partial \beta} + h_t\left(\frac{\partial \tau_a}{\partial \beta}\frac{\partial F_a}{\partial v} - \frac{\partial F_a}{\partial \beta}\frac{\partial \tau_a}{\partial v}\right) + k_{\tau_g}N_g\frac{\partial F_a}{\partial \beta}\right]s^2 + \frac{K_t}{h_t}\frac{\partial \tau_a}{\partial \beta}s \tag{27}$$

Hence the condition for NMPZ on $\beta \to \omega$ control is:

$$h_t^2\left(\frac{\partial F_a}{\partial v} - \left(\frac{\partial \tau_a}{\partial v} - k_{\tau_g}\frac{N_g}{h_t}\right)\frac{\frac{\partial F_a}{\partial \beta}}{\frac{\partial \tau_a}{\partial \beta}}\right) < -D_t \tag{28}$$

This corresponds with an operating point where τ_a *is rather influenced by* v *and* F_a *is rather influenced by* β. In presence of NMPZ, i.e. if eq. 28 is true, the sign of $d\omega$ depends on the choice of $d\ddot{\beta}$, $d\dot{\beta}$ and $d\beta$. Intuitively, the latter only happens when eq. 28 is verified: increasing blade pitch will *reduce* F_a *more than it increases* τ_a (because F_a *is rather influenced by* β), thus

210 $\dot{\phi}$ will decrease and cause relative wind $v_r = v - h_t\dot{\phi}$ to increase. As τ_a *is rather influenced by* v, this will reduce ω in the end. In practice, this effect can become an issue if a ω control algorithm obtains the opposite result than what was expected.

Because of this issue, literature has concerned the NMPZ phenomenon on $\beta \rightarrow \omega$ control and suggested several control corrections. Due to the nature of this phenomenon, any correction concerning β control, introduced in eq. 13, can't prevent this NMPZ. However, detuning the PI controller (by lowering k_P and k_I gains) or using the β platform pitch compensation

215 $d\beta_{comp} = k_\beta\dot{\phi}$ as suggested in (Abbas et al., 2021), can mitigate the effect of NMPZ when eq. 28 is true.

However, the complete prevention of the problem can be obtained by several set of parameters that involves both the WTG, the floating platform and the control set-up. In fact, for this NMPZ, equation 14 of the control model described in Section 2.1 allows one to avoid NMPZ by choosing a well-suited value of k_{τ_g}. This compensation has been already introduced by Stockhouse et al. (2021) with the formula:

220
$$k_{\tau_g} = m_{\tau_g}\frac{h_t}{N_g}\frac{\partial\tau_a}{\partial v}, \quad m_{\tau_g} \in [0,1] \tag{29}$$

The authors notice however it usually needs to be saturated because of turbine generator design constraints.

In absence of NMPZ, i.e. eq. 28 being false, increasing β from a steady-state operating point will always imply reducing ω. In order to visualize this NMPZ, Figure 3 shows ω responses to a β-step input (at $t = 10s$). On the left, parameters (Table 2) are chosen so that the condition eq. 28 is false: ω decreases. On the right, parameters are chosen so that condition eq. 28 is true:

225 at first ω increases even though β has step up.

Table 2. Set of parameters to show the NMPZ of eq. 28

	eq. 28 false	eq. 28 true
$\frac{\partial\tau_a}{\partial v}$	$2980.9\ kN.s$	$2838\ kN.s$
$\frac{\partial F_a}{\partial v}$	$354.8\ kN.s.m^{-1}$	$303.0\ kN.s.m^{-1}$
$\frac{\partial\tau_a}{\partial\omega}$	$-58597.1\ kN.m.s.rad^{-1}$	$-59428.7\ kN.m.s.rad^{-1}$
$\frac{\partial F_a}{\partial\omega}$	$-5658.0\ kN.s.rad^{-1}$	$-6282.9\ kN.s.rad^{-1}$
$\frac{\partial\tau_a}{\partial\beta}$	$-152347.8\ kN.m.rad$	$-133058.7\ kN.m.rad$
$\frac{\partial F_a}{\partial\beta}$	$-16052.2\ kN.rad$	$-18247.0\ kN.rad$
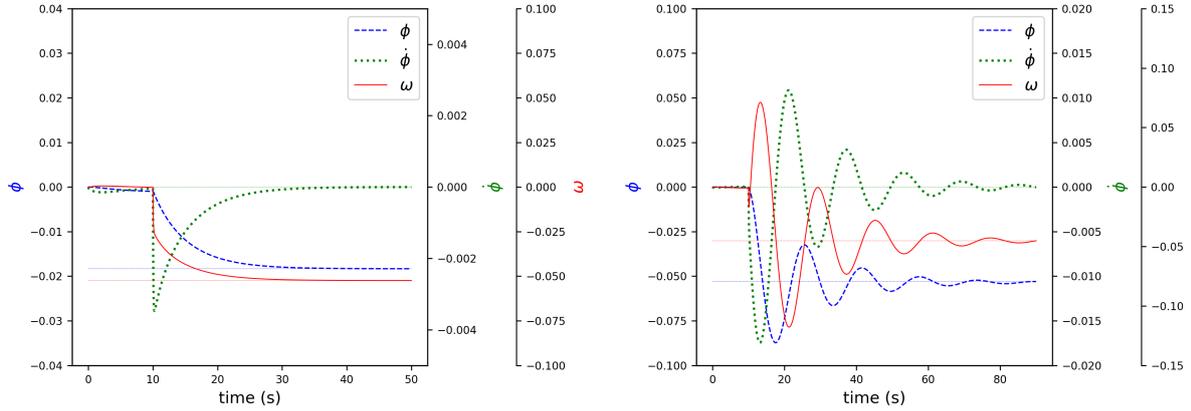
Figure 3. ω responses to a β-step input (at $t = 10s$). On the left, parameters (Table 2) are chosen so that the condition eq. 28 is false: ω decreases. On the right, parameters are chosen so that condition eq. 28 is true: at first ω increases even though β has step up.

2.3.3 Conclusion of NMPZ analysis:

Comparison between Figures 2 and 3 enlightens what really happens after a step input, with and without NMPZ: at the beginning both ω and $\dot{\phi}$ always decrease just after the step. However, when both NMPZ conditions eq. 25 and eq. 28 are false, those tendencies don't change. Conversely, when eq. 25 is true, we observe that $|\dot{\omega}|$ is so big that $\dot{\phi}$ jumps into positive values. 230 Similarly, when eq. 28 is true, we observe that $|\dot{\phi}|$ is so big that ω jumps (only for a short time) into positive values. NMPZ, as we have seen in the examples, can cause important shifts and unexpected behaviors for both ω and ϕ.

The NMPZ $\beta \rightarrow \phi$ doesn't depend on above defined parameters: the model in Section 2.1 does not give solution to always prevent it, but condition eq. 25 forecasts which operating points it affects. On the other hand, a wise choice of τ_g avoids $\beta \rightarrow \omega$ NMPZ, which is the main reason why this compensation has already been introduced by Stockhouse et al. (2021) and in the 235 control model in Section 2.1.

In order to complete the analysis of NMPZ phenomena related to FOWT system, a hypothetical situation where both conditions eq. 25 and eq. 28 are true has been simulated and reported in Figure 4. At first, the dynamics are always the same: both $\dot{\phi}$ and ω decrease, but soon they both diverge because of the negative damping. It is to be noted that, k_P/k_I corrections (without compensations τ_g and k_β) can delay this divergence but can not avoid it.

Table 3. Set of parameters to show the instability given by NMPZs of eq. 25 and eq. 28.

	eq. 25 and eq. 28 true
$\frac{\partial \tau_a}{\partial v}$	$3105.0\ kN.s$
$\frac{\partial F_a}{\partial v}$	$293.0\ kN.s.m^{-1}$
$\frac{\partial \tau_a}{\partial \omega}$	$-51356.5\ kN.m.s.rad^{-1}$
$\frac{\partial F_a}{\partial \omega}$	$-7150.0\ kN.s.rad^{-1}$
$\frac{\partial \tau_a}{\partial \beta}$	$-148063.0\ kN.m.rad$
$\frac{\partial F_a}{\partial \beta}$	$-16543.6\ kN.rad$
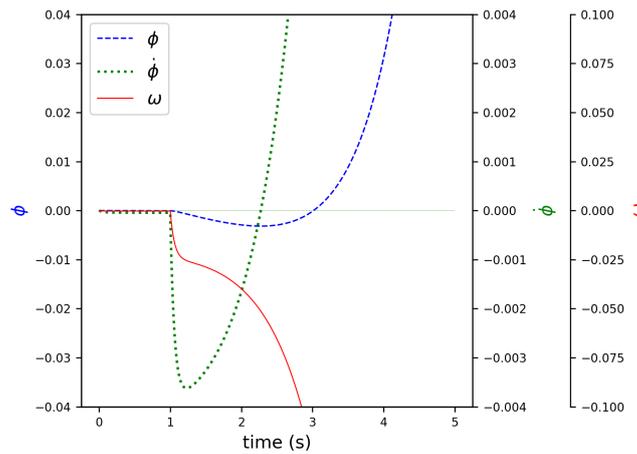
Figure 4. an hypothetical situation where both conditions eq. 25 and eq. 28 are true. At first, both $\dot{\phi}$ and ω decrease, but soon they both diverge because of the negative damping (k_P/k_I corrections can delay this divergence but can not avoid it).

2.4 Damping analysis

In section 2.3 the issue of NMPZ, ie. the issue of negative damping in the *control/input side* of the equation, is analysed. The influence of the gains k_P, k_I, k_β and k_{τ_g} on the damping of the system (cf. Section 2.3) is investigated within the analytical framework set in the previous sections. The goal is to optimize (or tune) the stability of ω and ϕ responses to an external (v and w) disturbance. In other words, the goal is to obtain an explicit expression of the damping of the FOWT system with respect to the control parameters, k_P, k_I, k_β and k_{τ_g}, such that, for an imposed level of damping, one can obtain a value of the control parameters. This is a powerful result for the floating wind community and a novelty of this work with respect to the existing literature.

Considering the whole system, with both degrees of freedom ω and ϕ and their coupling, $\chi_A(s)$ of equation 18 in the complex domain leads to the equation 21. The study of the damping is related to $\chi_A(s) = det(sI - A)$. The explicit form of χ_A is:

$$\chi_A(s) = \chi_{rot}(s)\chi_{plt}(s) + \frac{N_g h_t}{J_r J_t} s \left[(k_p s + k_I)\frac{\partial F_a}{\partial \beta}h_t\frac{\partial \tau_a}{\partial v} - \left(\frac{J_r}{N_g}\frac{\partial F_a}{\partial \beta}(k_P s + k_I) + \frac{\partial F_a}{\partial \omega} \right)\left(k_\beta\frac{\partial \tau_a}{\partial \beta} + k_{\tau_g}N_g \right) \right] \tag{30}$$

where:

$$\chi_{rot}(s) = s^2 - \frac{N_g}{J_r}\frac{\partial \tau_a}{\partial \omega}s - \frac{N_g}{J_r}\frac{\partial \tau_a}{\partial \beta}(k_P s + k_I)$$

$$\chi_{plt}(s) = s^2 + \frac{1}{J_t}(D_t + h_t^2\frac{\partial F_a}{\partial v} + k_\beta h_t\frac{\partial F_a}{\partial \beta})s + \frac{K_t}{J_t} \tag{31}$$

The term in square parenthesis represents the coupling term between the dynamics of the platform (ϕ) and the dynamics of the rotor (ω).

In this coupled form, it is complicated to explicit the damping of the system. In the next paragraph, under some hypothesis, the coupled system can be separated in two second order systems, one related to the rotor dynamics ω and the other one related to the floating dynamics ϕ. In particular, for the latter, it is possible to define a damping for the floating platform and obtain an explicit form for the compensation term k_β related to the imposed damping.

2.4.1 Simplified analysis of rotor dynamics:

Defining a damping coefficient (or a damping ratio) requires to reduce the global system to a second order oscillatory system. Equations 16 couples rotor and platform pitch dynamics, they hence involve a 4th order polynomial expression. In order to deal with rotor dynamics independently of the platform, it is supposed:

$$h_t\dot{\phi} \ll v \tag{32}$$

For large FOWT systems, this hypothesis is, generally, respected. It implies:

$$N_g k_{\tau_g}\dot{\phi} \ll \frac{\partial \tau_a}{\partial v}v$$

$$\frac{\partial \tau_a}{\partial \beta}k_\beta\dot{\phi} \ll \frac{\partial \tau_a}{\partial v}v \tag{33}$$

Under such assumption, the linear form of equation 1 becomes:

$$\dot{\omega} = \frac{N_g}{J_r}\left(\frac{\partial \tau_a}{\partial \omega}\omega + \frac{\partial \tau_a}{\partial v}v + \frac{\partial \tau_a}{\partial \beta}\beta - \tau_g \right) \tag{1''}$$

and the control is described by the PI controller: $\dot{\beta} = k_P\dot{\omega} + k_I\omega$, such that the resulting Laplace transform equation is

270   $$\underline{\omega}(s) = G_{rot}(s)\underline{v}(s) \tag{34}$$

where, considering a $k_I > 0$,

$$G_{rot}(s) = \frac{\frac{\partial\tau_a}{\partial v}s}{s^2 - \frac{N_g}{J_r}\frac{\partial\tau_a}{\partial\omega}s - \frac{N_g}{J_r}\frac{\partial\tau_a}{\partial\beta}(k_Ps + k_I)},$$

i.e. $$G_{rot}(j\nu) = \frac{1}{1 + \frac{j}{2\zeta_{rot}}\left(\frac{\nu}{\nu_{rot}} - \frac{\nu_{rot}}{\nu}\right)}\frac{-\frac{\partial\tau_a}{\partial v}}{\frac{N_g}{J_r}\frac{\partial\tau_a}{\partial\omega} + \frac{N_g}{J_r}\frac{\partial\tau_a}{\partial\beta}k_P} \tag{35}$$

with:

$$\nu_{rot} = \sqrt{-\frac{N_g}{J_r}\frac{\partial\tau_a}{\partial\beta}k_I}\,, \quad \zeta_{rot} = -\frac{\frac{N_g}{J_r}\frac{\partial\tau_a}{\partial\omega} + \frac{N_g}{J_r}\frac{\partial\tau_a}{\partial\beta}k_P}{2\sqrt{-\frac{N_g}{J_r}\frac{\partial\tau_a}{\partial\beta}k_I}} \tag{36}$$

275   Thus, when all interactions with platform pitch are neglected, the rotor behaves like a second order oscillatory system. The corresponding filter G_{rot} is a second order band-pass filter with cutoff angular frequency ν_{rot} [1].

The above formulas enable one to obtain explicitly k_I and k_P.

They are well known: several controllers, such as ROSCO (Abbas et al., 2021), suggest to define:

$$|k_I| = \left|\frac{\nu_{rot}^2}{\frac{N_g}{J_r}\frac{\partial\tau_a}{\partial\beta}}\right| \quad \text{and} \quad |k_P| = \left|\frac{\left(\frac{N_g}{J_r}\frac{\partial\tau_a}{\partial\omega} + 2\zeta_{rot}\nu_{rot}\right)}{\frac{N_g}{J_r}\frac{\partial\tau_a}{\partial\beta}}\right| \tag{37}$$

280   ### 2.4.2   Simplified analysis of platform dynamics:

Similarly to what is done in the previous paragraph, here the global system 1 is reduced to a second order oscillatory system that allows us to have a better understanding of platform dynamics.

Considering $k_P = k_I = 0$ and assuming:

$$\frac{\partial F_a}{\partial\omega}\omega << \frac{\partial F_a}{\partial v}v_r + \frac{\partial F_a}{\partial\beta}\beta \tag{38}$$

285   The latter is the condition to decouple the global system. It enables to consider ϕ response independently of ω, and as a second order oscillatory system's degree of freedom. The resulting Laplace transform equation is:

$$\begin{pmatrix}\phi \\ \dot{\phi}\end{pmatrix}(s) = G_{plt}(s)\underline{u}_d(s) \tag{39}$$

$u_d = \begin{pmatrix} v \\ w \end{pmatrix}$: the input array is reduced because only the damping in the *output side* is analysed and it is not necessary for this to consider any additional control input.

290   $$G_{plt}(s) = (sI - A_{plt})^{-1}B_d \tag{40}$$

---

[1]In case $k_I \leq 0$, ν_{rot} and ζ_{rot} would be imaginary according to the formulas above. G_{rot} would be no longer a band-pass filter.

$$A_{plt} = \begin{bmatrix} 0 & 1 \\ -\frac{K_t}{J_t} & \frac{-1}{J_t}(D_t + h_t^2 \frac{\partial F_a}{\partial v} + k_\beta h_t \frac{\partial F_a}{\partial \beta}) \end{bmatrix} \tag{41}$$

A_{plt} is the bottom-right part of A defined in 17.

Looking at the ϕ degree of freedom, eq. 39 gives:

$$\underline{\phi}(s) = G_{plt,1,1}(s)\underline{v}(s) + G_{plt,1,2}(s)\underline{w}(s), \tag{42}$$

with:

$$(G_{plt,1,1}, G_{plt,1,2})(s) = \left(\frac{\frac{h_t}{J_t}\frac{\partial F_a}{\partial v}}{s^2 + \frac{1}{J_t}(D_t + h_t^2\frac{\partial F_a}{\partial v} + k_\beta h_t \frac{\partial F_a}{\partial \beta})s + \frac{K_t}{J_t}}, \frac{\frac{1}{J_t}\frac{\partial \tau_w}{\partial w}}{s^2 + \frac{1}{J_t}(D_t + h_t^2\frac{\partial F_a}{\partial v} + k_\beta h_t \frac{\partial F_a}{\partial \beta})s + \frac{K_t}{J_t}} \right), \tag{43}$$

i.e.:

$$(G_{plt,1,1}, G_{plt,1,2})(j\nu) = \frac{1}{1 - \left(\frac{\nu}{\nu_{plt}}\right)^2 + 2j\zeta_{plt}\frac{\nu}{\nu_{plt}}} \left(\frac{h_t}{K_t}\frac{\partial F_a}{\partial v}, \frac{1}{K_t}\frac{\partial \tau_w}{\partial w} \right), \tag{44}$$

$$\nu_{plt} = \sqrt{\frac{K_t}{J_t}}, \qquad \zeta_{plt} = \frac{1}{2\sqrt{K_t J_t}}\left(D_t + h_t^2 \frac{\partial F_a}{\partial v} + k_\beta h_t \frac{\partial F_a}{\partial \beta} \right) \tag{45}$$

Thus, when all interactions with rotor dynamics are neglected, the platform behaves like a second order oscillatory system. The corresponding filter G_{plt} is a second order low-pass filter with cutoff angular frequency defined by ν_{plt} and damping ratio defined by ζ_{plt}.

2.5 Artificial damping of the platform : ζ_{plt}-fixed strategy

By knowing the features of the FOWT, one can impose a given level of damping and obtain an explicit expression for the k_β:

$$k_\beta = \frac{1}{h_t\frac{\partial F_a}{\partial \beta}}\left(2\sqrt{K_t J_t}\zeta_{plt} - D_t - h_t^2\frac{\partial F_a}{\partial v} \right) \tag{46}$$

The strategy is such that k_β is a negative number instead of what is proposed in the literature. In (Stockhouse et al., 2021), $\beta_{comp} = -k_\beta \dot{\phi}$ is introduced in order to erase at first order the coupling between platform and rotor dynamics, and therefore k_β is positive, defined by:

$$k_\beta = -h_t\frac{\partial \tau_a}{\partial v} \Big/ \frac{\partial \tau_a}{\partial \beta} \tag{47}$$

²

---

²In (Abbas et al., 2021), β_{comp} is defined as in (Stockhouse et al., 2021) but with the convention $\beta_{comp} = k_{float}\dot{\phi}$ so that $k_{float} = -k_\beta = h_t\frac{\partial \tau_a}{\partial v}\Big/\frac{\partial \tau_a}{\partial \beta}$ is negative.

2.5.1 Expected effect on platform dynamics

Figure 5 shows the second order low-pass filter G_{plt}. In other words, it is how ζ_{plt} value can affect the damping of platform oscillations.

315   It can be observed that ζ_{plt} has a significant effect on the damping of platform oscillations only for angular frequencies $\nu \approx \nu_{plt,natural}$. Yellow vertical band in figure 5 shows the interval of angular frequencies I_{damped}, arbitrarily defined by:

$$I_{damped} = \left[\frac{\nu_{plt,natural}}{\sqrt{2}} \ , \ \sqrt{2}\nu_{plt,natural} \right] \tag{48}$$

that are directly damped when ζ_{plt} increases. Therefore, it is to be expected that ζ_{plt}-fixed strategy will be well fit to reduce platform motion and tower loads when their variations happen at an angular frequency $\nu \in I_{damped}$.
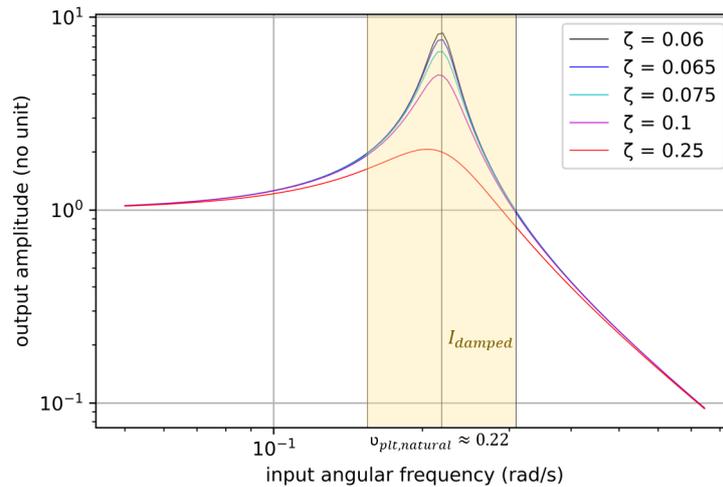
Figure 5. Bode diagram of second order low-pass filter G_{plt}

320   2.5.2 Expected effect on rotor dynamics

In this part the first order effect of ζ_{plt}-fixed strategy on the rotor dynamics is analysed. The state space representation of the FOWT dynamics is given by equation 16. By considering 0 input (ie. $u_{c,ol} = u_d = 0$), this leads to the following linear equation, truncated at first order:

$$\dot{\omega} = \ddot{\theta} = A_{2,1}\theta + A_{2,2}\dot{\theta} + A_{2,4}\dot{\phi}, \tag{49}$$

325   where

$$
\begin{aligned}
A_{2,4} &= \frac{N_g}{J_r} \left(-h_t \frac{\partial \tau_a}{\partial v} - k_\beta \frac{\partial \tau_a}{\partial \beta} + k_{\tau_g} N_g \right) \\
&= \frac{N_g}{J_r} \left(-h_t \frac{\partial \tau_a}{\partial v} + \frac{\frac{\partial \tau_a}{\partial \beta}}{h_t \frac{\partial F_a}{\partial \beta}} \left(D_t + h_t^2 \frac{\partial F_a}{\partial v} - 2\sqrt{K_t J_t}\zeta_{plt} \right) + k_{\tau_g} N_g \right).
\end{aligned}
\tag{50}
$$

Moreover, the following inequalities are verified for an above-rated operating point:

$$h_t \frac{\partial \tau_a}{\partial v} - k_{\tau_g} N_g \geq 0$$

$$\frac{\frac{\partial \tau_a}{\partial \beta}}{\frac{\partial F_a}{\partial \beta}} > 0$$

$$\frac{1}{2\sqrt{K_t J_t}} \left(D_t + h_t^2 \frac{\partial F_a}{\partial v} \right) \leq \zeta_{plt} \tag{51}$$

First inequality comes from 29 (notice that in section 3, it is considered $\tau_g = 0$). Third inequality is a consequence of the
330   assumption that ζ_{plt}-fixed strategy aims at increasing the damping of the platform. This implies that:

$$\frac{\partial}{\partial \zeta_{plt}} |A_{2,4}| > 0 \tag{52}$$

meaning that the first order coupling between platform dynamics and rotor dynamics will increase when ζ_{plt} increases if
ζ_{plt}-fixed strategy is applied. Thus, if the characteristic time of platform dynamics is small enough, the equation truncated at
first order is valid and it is to be expected that, at least for some tunings of the PI controler, ζ_{plt}-fixed strategy would increase
335   rotor speed variations.

3   Numerical tests with time domain simulations

In this section, it is analysed how the new control strategy described in the previous section affects platform and rotor dynamics,
and especially the impact on tower loads and rotational speed. The *reference* is the control strategy without compensation, with
$k_\beta = 0$.
340   The ζ_{plt}-fixed strategy has been implemented in the ROSCO environment (ROSCO, 2021), replacing the existing pitch
control. The rest of the controller remains basically the same. In the next, ζ_{plt}-fixed strategy is compared to the one without
compensation, named *reference*. The only difference between the two terms of comparison concerns the k_β. For the ζ_{plt}-fixed
strategy, it is given by 45. For the reference, it is $k_\beta = 0$.

3.1   Test cases

345   The simulation tool used is OpenFast v2.4.0 (https://github.com/OpenFAST/openfast) and the FOWT model considered is the
IEA 15 MW wind turbine mounted over the UMaine VolturnUS-S semi-submersible floater (Allen et al., 2020). Initially simple
constant wind and monochromatic waves are testes in order to verify the analytical developments of the previous section. Then
a test case more representative of the industrial design of FOWT is considered by testing a DLC1.1. For the latter, simulation
consider only 1 seed of 3600 seconds with aligned wind and irregular waves. For this time simulation, this is statistically
350   equivalent to 600 seconds and 6 seeds.

3.2 Tuning of the PI controller

Values of k_P, k_I, k_β are continuously updated following the explicit expression given in equations 36 and 45, then low-pass filtered. This means that globally, for each of these test cases and each set of parameters, k_P, k_I, k_β have almost fixed values. After some tests, for all the considered simulations, $\zeta_{rot} = 0.6$ and $\nu_{rot} = 0.01$ are chosen for the PI controller's tuning. This choice ensures that most of the wave spectrum (which peaks at $T \approx 11 \ s$, ie. $\nu \approx 0.57 \ rads^{-1}$) and platform dynamics natural angular frequency ($\nu_{plt} \approx 0.22 \ rad.s^{-1}$) fall outside of G_{rot} pass-band. In the next sections, several values of platform damping are analyzed for the ζ_{plt}-fixed strategy and compared to the reference strategy for different test case.

3.3 Still wind and monochromatic wave

For the still wind and monochromatic wave condition, two ζ_{plt} are tested: $\zeta_{plt} = 0.1$ and $\zeta_{plt} = 0.25$. The corresponding quality factors are: $Q = 5$ and $Q = 2$, respectively. Thus, the platform is expected to behave like an under-damped second order oscillatory system. Table 6 states external conditions for test cases with still wind and monochromatic wave. Hereafter, results are plotted over time are drawn for a 100 seconds time interval in a simulation on a long period of time, so that the operating point is reached. When necessary for a better understanding, results are reported for a longer interval.

Table 4. Environmental conditions for the numerical test cases.

case	wind speed V (ms^{-1})	wave period Tp (s)	wave height H_w (m)
(1)	11	11	1.5
(2)	11	28.75	1.5
(3)	22	11	1.5
(4)	22	28.75	1.5

Table 5 gives the mean value of k_β for test cases (1) to (4). Cases (1), (2) and cases (3), (4) are gathered together as they use the same mean value of k_β.

Table 5. compensation gain (k_β).

case	$\zeta_{plt} = 0.10$	$\zeta_{plt} = 0.25$	reference
(1) and (2)	$k_\beta = -8.6$	$k_\beta = -42.7$	$k_\beta = 0.0$
(3) and (4)	$k_\beta = -7.4$	$k_\beta = -34.8$	$k_\beta = 0.0$
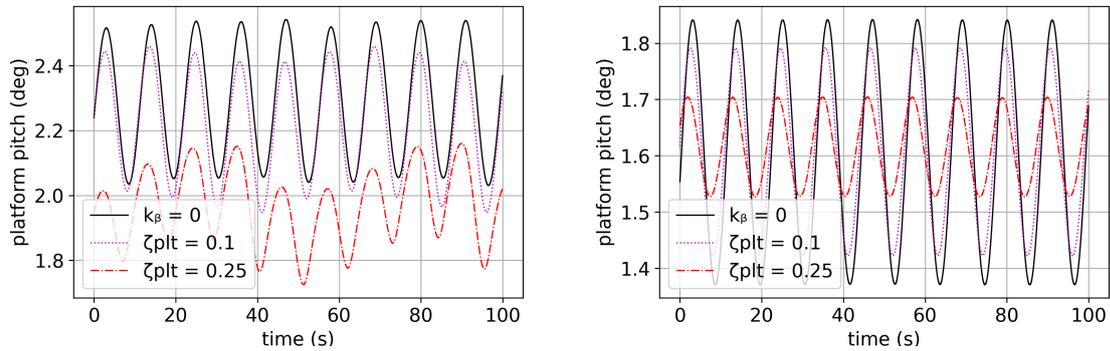
Figure 6. Platform pitch Φ (deg) for a monochromatic wave of period 11s (test case (1) on the left and (3) on the right).
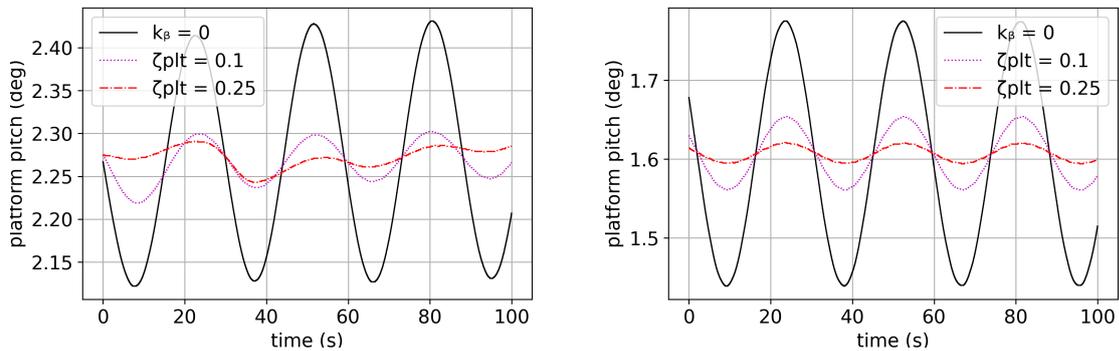
Figure 7. Platform pitch Φ (deg) for a monochromatic wave of period 28.75s (test case (2) on the left and (4) on the right).

Figures 6 and 7 show the forced oscillations of the platform when it is subjected to a monochromatic wave of period $11s$ (which corresponds to the realistic fundamental period of a wave) and $28.75s$ (which is the natural period of the platform). As shown by the analytical development, increasing ζ_{plt} reduces platform oscillations, especially when the wave period is close

370 to the natural period of the platform (see diagram 5). This is shown in Figures 8 and 9 where the density of occurrence of each value of tower bottom reaction moment is reported. For the monochromatic wave with period $11s$ the damping of the ζ_{plt}-fixed strategy is less evident. More floating wind test cases are reported in the next section.
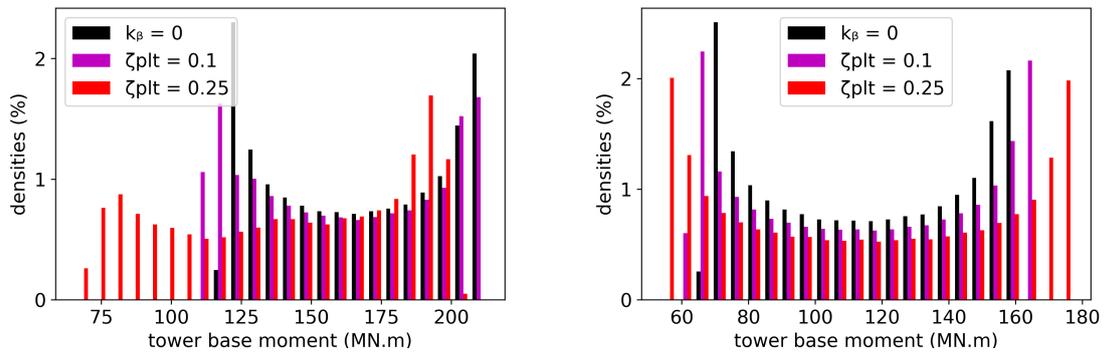
Figure 8. Tower base moment (MN.m) densities for a monochromatic wave of period 11s (test case (1) on the left and (3) on the right).
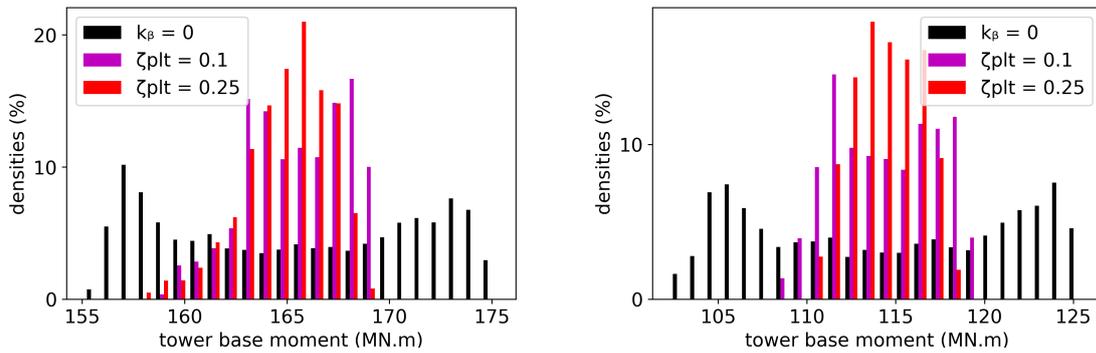
Figure 9. Tower base moment (MN.m) densities for a monochromatic wave of period 28.75s (test case (2) on the left and (4) on the right).
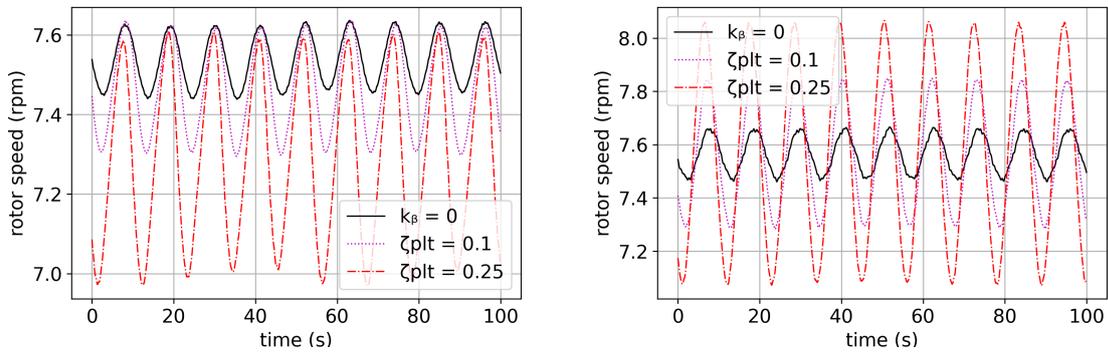
Figure 10. Rotor speed (rpm) evolution over time for test cases (1) on the left and (2) on the right
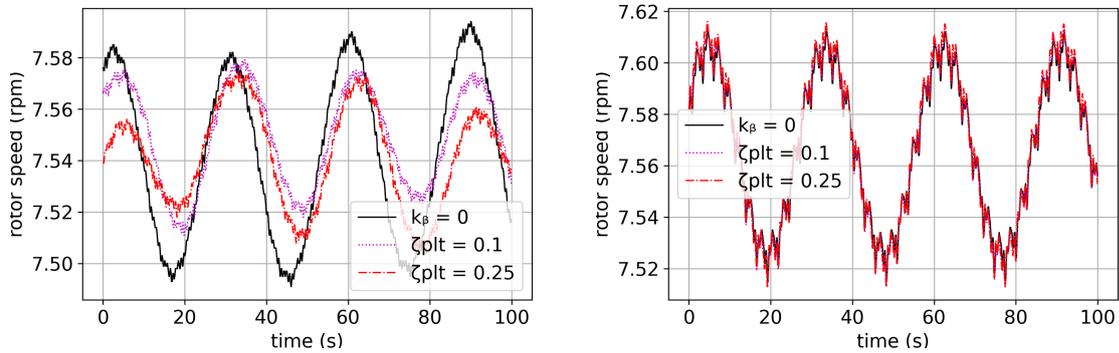
Figure 11. Rotor speed (rpm) evolution over time for test cases (3) on the left and (4) on the right.

ζ_{plt}-fixed strategy's effect on rotor dynamics is not easily described by a second order linear equation: it involves the coupling between platform and rotor dynamics, which was analysed at first order in 2.5. From this analysis, ζ_{plt}-fixed strategy was

375   expected to increase the coupling between platform and rotor dynamics for a short characteristic time. In Figure 10 and 11 it can be observed that for a short characteristic time ($11s$) ζ_{plt}-fixed strategy increases rotor speed variations, but not for a longer characteristic time, such as $28.75s$ (for which it behaves slightly better than $k_\beta = 0$ strategy).

To conclude this part of the tests: β-compensation strategies perform very differently depending on the oscillatory frequency of the platform:

380   – For angular frequencies $\nu \in I_{damped} = \left[\frac{\nu_{plt,natural}}{\sqrt{2}} \ , \ \sqrt{2}\nu_{plt,natural} \right]$, ζ_{plt}-fixed strategy is very effective when it comes to the damping of platform oscillations, as seen in paragraph 2.5 (cf. figure 5). The tests highlight that ζ_{plt}-fixed strategy is reducing both tower loads and rotor speed variations in turbulent wind conditions.

– For angular frequencies outside the previous set, ζ_{plt}-fixed strategy is less effective for damping platform oscillations. Tower loads reduction by ζ_{plt}-fixed strategy is therefore barely visible, whereas rotor speed variations are actually am-
385   plified, especially when comparing this strategy to reference strategy.

3.4 DLC1.2 tests

Tests presented hereafter are more representative of what is done during design or verification of offshore wind structure. They are inspired by the DLC 1.2, for normal power production in normal turbulence and normal sea state, as described in IEC standards. This kind of load case aim at assessing the fatigue design criteria. Kaimal's turbulence model is considered
390   following IEC 61400 v.3 for a Wind Turbine of turbulence type B, for average wind speeds from $12 \ ms^{-1}$ to $24 \ ms^{-1}$, as described in Table 6. The wind box is generated by TurbSim tool developed by NREL. For the waves, JONSWAP distributions are considered with significant wave height $Hs = 1.5m$, wave period $Tp = 11.0s$ and $\gamma = 2.0$. Wind and waves are considered aligned in the same direction. All the degrees of freedom of the floating platform are allowed, including the surge motion. In other terms, the numerical twin reproduces, with the accuracy of the chosen model, the actual motion of the FOWT. Tower and

395 blades are fully deformable. As already done for the previous test cases, the ζ_{plt}-fixed strategy is compared to the reference strategy, $k_\beta = 0$.

The level of damping imposed to the platform is ζ_{plt}-fixed = 0.1. This value is found to be the most interesting to be tested for this floater and WTG configuration. Other tests with higher values of imposed damping show less interesting results. The choice of the right ζ_{plt} for each FOWT system is important and demands for some iterations before concluding.

Table 6. Environmental conditions for DLC 1.2.

Time sim $[s]$	w.speed $[m.s^{-1}]$	w. condition	Tp $[s]$	H_s $[m]$	γ	waves dir.
3600	$12.0 - 24.0$	Normal turbulence B	11.0	1.5	2.0	co-linear
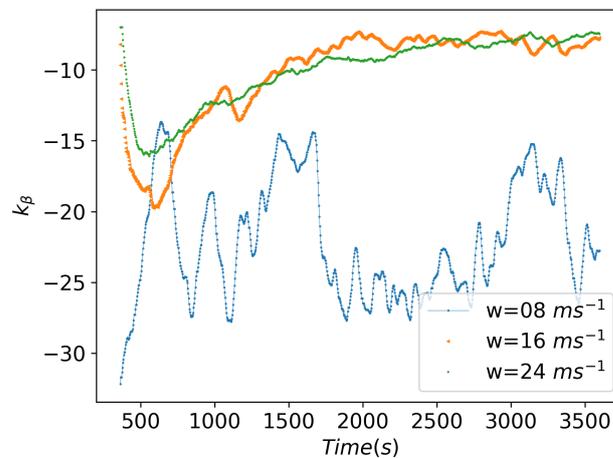
Figure 12. evolution of k_β for some of the simulations.

400 Figure 12 shows how k_β evolves for some cases of the simulation pool. The below-rated behaviour is more dynamic than the over-rated, where the floating feedback is more stable. As remarked in 2.5, the k_β for the ζ_{plt}-fixed is a negative value.

From the time series of the tower bottom moment, a rainflow algorithm is used to count the cycles following ASTM normative (ASTM, 2017). The DEL is obtained by using a Wohler's curve with a single slope of exponent $m = 3.0$. Platform pitch, power, rotor speed, blade pitch, tower load and tower DEL results of the simulations for the comparison are resumed in Figure 405 13. The ζ_{plt}-fixed strategy reduces platform pitch motion for all wind speeds. As expected this is done by the coupling with the rotor and the use of the blade pitch. The increase in the average value of the pitch explains the slight decrease in rotor speed for the above rated wind speeds. The generator power is also affected, slightly increased for lower wind speeds and slightly decreased for higher wind speeds (around $+/-1\%$).

Loads in the tower are reduced and fatigue Design Equivalent Load (DEL) also. This is remarkable for around rated speed.
For high wind speeds, the gain is less evident. In average there is a gain around 15% of the DEL. Table 7 shows, for the 10 ms^{-1} case, a deeper comparison by reporting the statistics of the quantities of interest extracted from this simulation. The difference in the minimum value of the moment at the tower base is remarkable: passing from $80.97~MNm$ for the reference up to $165.40~MNm$ for the ζ_{plt}-fixed strategy. This is also clear in the difference of the standard deviations. The amplitudes of the oscillations of this load are reduced.

It is interesting to analyse Figure 14. This figure reports a deeper analysis of the fatigue damage. In fact, the stress in the tower bottom section is obtained by considering the design proposed by UMaine in (Allen et al., 2020). Then, an offshore Wohler's curve is considered with two slopes in the log-log domain: $m = 3.0$ for loads with less than 1.0 million cycles and $m = 5.0$ for loads with higher number of cycles. Those are typical values proposed by DNV for offshore steel structures. This analysis leads to obtain an estimation of the 25 years damage at the tower bottom. The gain is much more evident than the DEL. This is due to the second slope, $m = 5.0$, which amplifies the changes in the load amplitudes. Offshore WTG in production are mostly subjected to a very high number of cycles of small amplitudes. This figure shows also the effect of the turbulence on the fatigue. In fact, looking at the reference, up to $12~ms^{-1}$, the shape of the damage distribution follows the one of the thrust curve. However, since the turbulence is a percentage of the average wind speed, from $16~ms^{-1}$, the damage starts increasing again.

Table 7. Statistics for results concerning the case with mean wind speed at $10~ms^{-1}$. For each quantity of interest, there is the comparison of the minimum, maximum, mean and standard deviation values produced by the ζ_{plt}-fixed control strategy and the reference.

	$\zeta_{plt} = 0.1$ min	$k_\beta = 0$ min	$\zeta_{plt} = 0.1$ mean	$k_\beta = 0$ mean	$\zeta_{plt} = 0.1$ max	$k_\beta = 0$ max	$\zeta_{plt} = 0.1$ st.d.	$k_\beta = 0$ st.d
PtfmPitch [deg]	2.84	1.09	4.55	4.56	5.62	5.91	0.51	0.59
TwrBsM [MNm]	165.40	80.97	366.66	367.79	493.80	505.10	43.20	46.82
GenPwr [MW]	7.85	5.49	12.09	12.01	15.15	15.19	1.29	1.47
BldPitch [deg]	0	0	0.218	0.176	6.651	8.33	0.394	0.729
RotSpeed [rpm]	5.23	5.34	6.90	6.92	7.90	8.00	0.61	0.60

The coupling between platform pitch and rotor dynamics is increased. Hence, an increase in the pitch utilization is expected. A specific fatigue analysis of the pitch bearing is realized by following (Shan et al., 2021), where three methods to evaluate the fatigue of the pitch bearing are compared leading to comparable results. The second method is implemented here in order to quantify the increment in the pitch fatigue caused by the ζ_{plt}-fixed strategy with respect to the reference. The bearing life is inversely proportional to the cube of the bearing loading. From the overturning moment acting on the bearing, the equivalent loading at N revolutions of the pitch bearing is given by:

$$M_{eq} = \left(\sum_i \frac{\Delta\beta_i \, M_i^3}{N} \right)^{1/3} \tag{53}$$
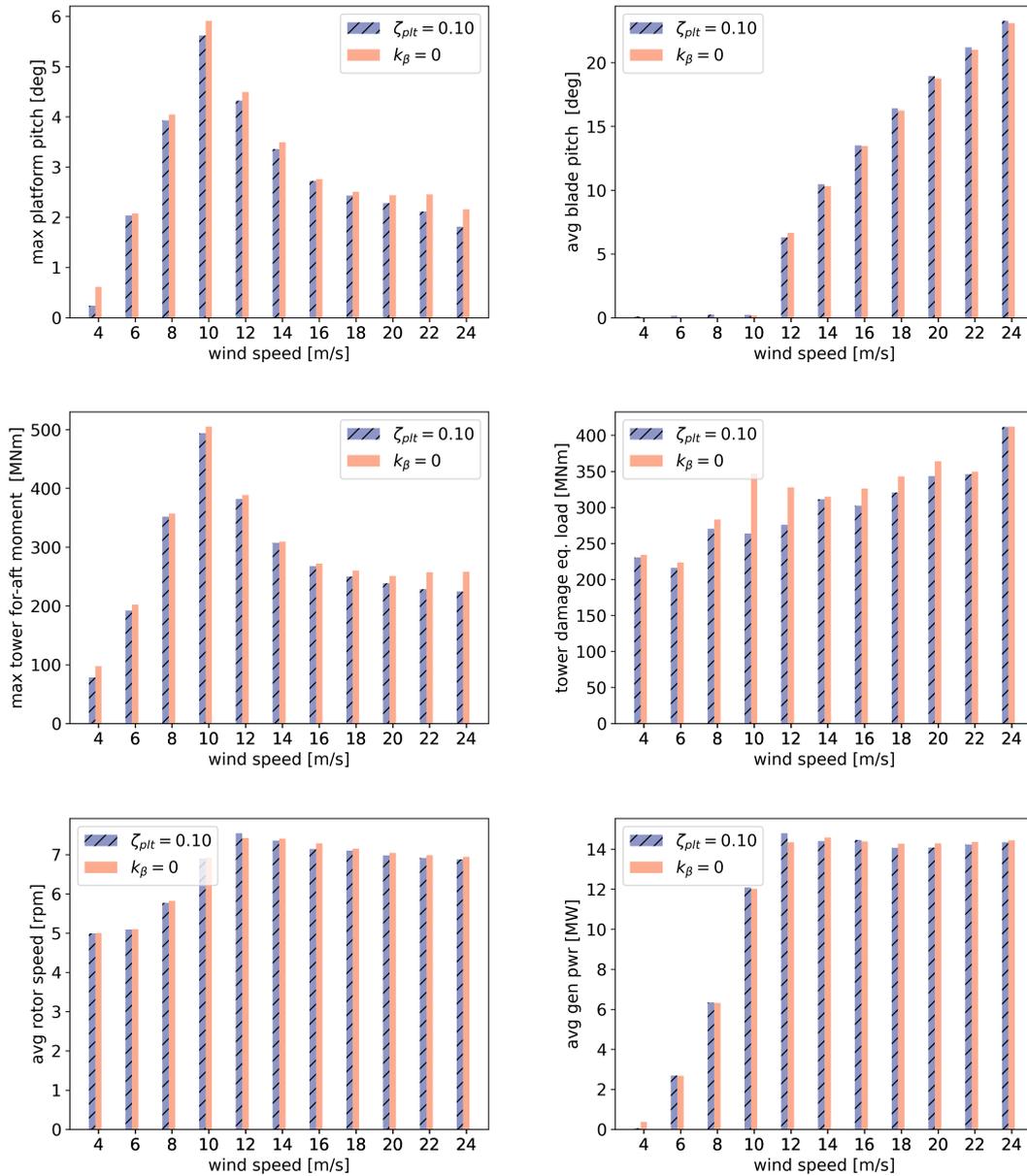
Figure 13. Comparison results for the DLC1.2 for the UMaine floater with IEA15MW WTG. The imposed level of damping in the platform dynamics for the ζ_{plt}-fixed strategy is 0.10. Outputs show statistics for platform pitch; blade pitch; Tower bending moment, max and damage equivalent load; rotor speed and generator power.

where i is the time step of the simulation. The discrete integral considers the product of the time series of the overturning moment M_i and the blade pitch variation $\Delta\beta_i$, over the entire simulation. To take into account the fact that, for each wind
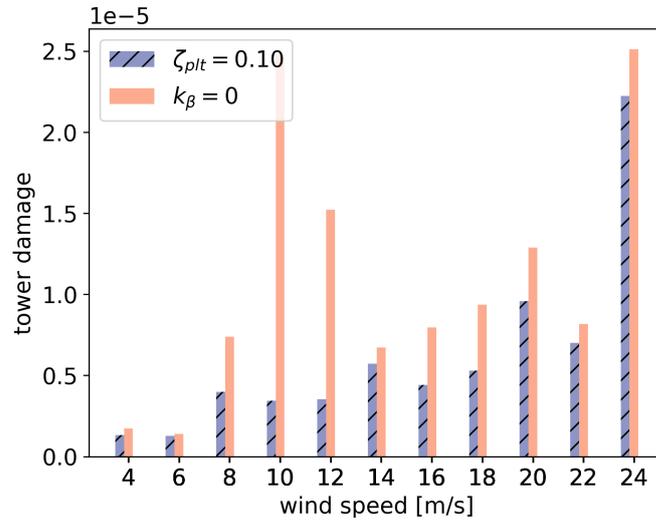
Figure 14. Fatigue cumulative damage at tower bottom by using rainflow counting and linear Miner's rule. The damage is obtained considering the tower base design proposed by the UMaine, a Wohler's curve bi-linear with $m = 3.0$ up to 10^6 cycles and $m = 5.0$ after, as proposed by DNV for Offshore steel. The probability of occurrence of each wind is equal, without any weibull distribution.

speed, the mean blade pitch is different, the 90 degrees of the pitch range are divided in 30 sectors, each one corresponding to

435   a different zone of the bearing. This corresponds to consider a tooth function in the integral of eq. 53 and it is well explained in Figure 11 of (Shan et al., 2021). In Figure 15, it is reported the increase in M_{eq} given by the ζ_{plt}-fixed strategy with respect to the reference. The increase in the use of the pitch bearing is estimated in a factor of 1.5 in average, with peaks of 2 around the rated wind speed. This is an aspect of the control strategy to be considered and it is an axis of improvement for future works.
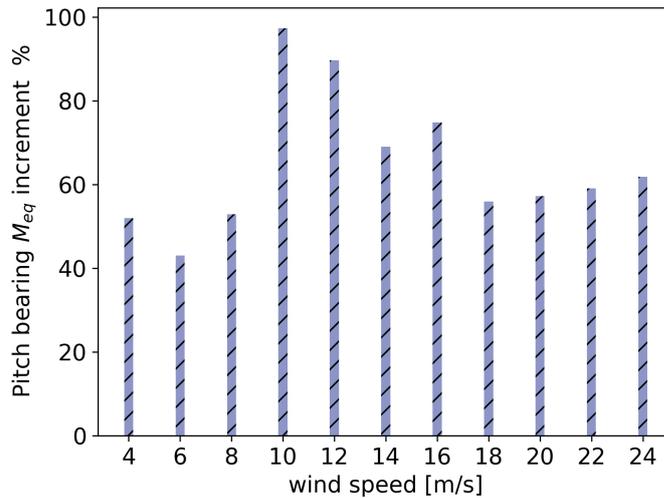
Figure 15. Increment in the use of the pitch bearing given by the ζ_{plt}-fixed strategy with respect to the reference. The increment is expressed in terms of % of M_{eq} (eq. 53)

4   Conclusions

440   The first part of this paper presents the analysis of the NMPZ related to the system of equations describing the dynamcs of a floating offshore wind turbine (FOWT). The equation of the rotor dynamics and the one of the platform dynamics are analysed in the complex domain to explicit the conditions leading to their respective NMPZs. One of those NMPZ, the instability given by the blade pitch on the rotor dynamics, is already known in literature and a compensation already exists to avoid it. The other one, the instability given by the blade pitch to the platform dynamics, is a novelty in the community. The effects of the

445   NMPZs are analysed on two analytical test cases: at the beginning both ω and $\dot{\phi}$ always converge to the right solutions just after the first steps. When both NMPZ conditions are not verified, those tendencies don't change. However, when the $\dot{\phi}$-NMPZ is verified, $|\omega|$ becomes so big that $\dot{\phi}$ jumps into unexpected values without converging to the expected solution. Similarly, when the ω-NMPZ condition is verified, $|\dot{\phi}|$ becomes so big that ω oscillates before converging to the expected solution. NMPZs can cause important shifts and unexpected behaviors for both ω and ϕ.

450   In the second part of the paper, the damping analysis is further investigated proposing a new strategy control for FOWT, named ζ_{plt}-fixed. This strategy is based on a compensation parameter k_β proportional to the platform pitch velocity. It considers the coupling between the rotor dynamics and the floating platform dynamics. The idea behind this control strategy is to activate the blade pitch to damp the platform motions. An explicit expression linking k_β to ζ_{plt} (damping ratio imposed to the platform) is obtained by deriving a second order filter from the equation of the platform dynamics.

455   This is different with respect to already existing strategies based on platform pitch compensation which aims at decoupling rotor and platform dynamics. This difference is underlined by the values of k_β, which is negative for the new control strategy,

while it is positive for the ones existing in literature. For each FOWT system, some iterations are necessary in order to find the optimum value for ζ_{plt}. The performances of the ζ_{plt}-fixed strategy are tested analytically and numerically by considering an OpenFAST numerical twin of the Umaine IEA15MW FOWT. For a test representative of the DLC1.2, the ζ_{plt}-fixed strategy

460   allows to reduce the loads at the tower foundation interface for all the considered wind speeds, without significant losses in terms of power production. The damage analysis shows a remarkable gain in terms of fatigue lifetime. The blade pitch use slightly increases remaining in the bounds of a standard controller limitations.

This work highlights the importance of defining proper controller strategies for FOWT in order to reduce loads on the structure or improve the performances and, then, it aims at helping the industry to achieve the objective in terms of LCOE

465   reduction.

Author contributions. Matteo Capaldo has contributed for the original idea of the new control strategy, the development of the numerical twin and the numerical tests and he is the main contributor for the paper editing. Paul Mella developed the mathematical framework, he has contributed for the original idea of the new control strategy and he has contributed for the paper editing

Competing interests. The authors declare there are not competing interests in this work.

References

Abbas, N., Zalkind, D., Pao, L. & A., W.: A Reference open-source controller for fixed and floating offshore wind turbines, Wind Energy Science, 7, 53–73, https://doi.org/10.5194/wes-7-53-2022, 2021.

Ali S., K., Li, Y., Nagamune, R., Zhou, Y. & Ur Rehman, W.: Platform motion minimization using model predictive control of a floating offshore wind turbine Theoretical And Applied Mechanics Letters, 11, https://doi.org/10.1016/j.taml.2021.100295, September 2021.

Allen, C., Viscelli, A., Dagher, H., Goupee, A., Gaertner, E., Abbas, N., Hall, M. & Barter, G.: Definition of the UMaine VolturnUS-S Reference Platform Developed for the IEA Wind 15-Megawatt Offshore Reference Wind Turbine, Golden, CO: National Renewable Energy Laboratory. NREL/TP-5000-76773., https://www.osti.gov/biblio/1660012, July 2020.

ASTM E1049-85, A. Standard Practices for Cycle Counting in Fatigue Analysis, https://www.astm.org/e1049-85r17.html, 2017

Bianchi, F., De Battista, H. & Mantz, R.: Wind Turbine Control Systems: Principles, Modelling and Gain Scheduling Design, ISBN: 978-1-84628-493-9, January 2007.

Jonkman, J.: Influence of Control on the Pitch Damping of a Floating Wind Turbine, NREL Report, https://www.nrel.gov/docs/fy08osti/42589.pdf, January 2008.

Fleming, P., Pineda, I., Rossetti, M., Wright, A. & Arora, D.: Evaluating Methods for Control of an Offshore Floating Turbine. Proceedings Of The International Conference On Offshore Mechanics And Arctic Engineering - OMAE. 9, https://doi.org/10.1115/OMAE2014-24107, June 2014.

Larsen, T. & Hanson, T.: A method to avoid negative damped low frequent tower vibrations for a floating, pitch controlled wind turbine, J. PHYS. CONF. SER.. 75 pp. 012073, https://iopscience.iop.org/article/10.1088/1742-6596/75/1/012073, August 2007.

Lackner, M.: Controlling Platform Motions and Reducing Blade Loads for Floating Wind Turbines. Wind Engineering. 33 pp. 541-554, https://doi.org/10.1260/0309-524X.33.6.5, December 2009.

Lee, J. & Zhao, F.: GWEC, Global Wind Report 2022, https://gwec.net/wp-content/uploads/2022/03/GWEC-GLOBAL-WIND-REPORT-2022.pdf, 2022.

Lenfest, E., Goupee, A., Wright, A.: & Abbas, N. Tuning of Nacelle Feedback Gains for Floating Wind Turbine Controllers Using a Two-DOF Model, https://doi:10.1115/OMAE2020-18770, August 2020.

Ma, Y. & Sclavounos, P.: Wave forecast and its application to the optimal control of offshore floating wind turbine for load mitigation, RENEW. ENERG.. 128 pp. 163-176, https://doi.org/10.1016/j.renene.2018.05.059, August 2018.

Menezes, E., Araújo, A., Rohatgi, J. & Foyo, P.: Active load control of large wind turbines using state-space methods and disturbance accommodating control, ENERGY. 150, https://doi.org/10.1016/j.energy.2018.02.143, February 2018.

Namik, H. & Stol, K.: Performance analysis of individual blade pitch control of offshore wind turbines on two floating platforms, Mechatronics. 21 pp. 691-703, https://doi.org/10.1016/j.mechatronics.2010.12.003, June 2011.

NREL ROSCO. Version 2.4.1. GitHub Repository, https://github.com/NREL/ROSCO, 2021.

Sarkar, S., Fitzgerald, B. & Basu, B.: Nonlinear model predictive control to reduce pitch actuation of floating offshore wind turbines, IFAC-PapersOnLine. 53 pp. 12783-12788, https://doi.org/10.1016/j.ifacol.2020.12.1936, January 2020.

Sarkar S., Chen L., Fitzgerald, B., Basu B.: Multi-resolution wavelet pitch controller for spar-type floating offshore wind turbines including wave-current interactions, Journal of Sound and Vibration 470, 115170, https://doi.org/10.1016/j.jsv.2020.115170, 2020

Schlipf, D., Sandner, F., Raach, S., Matha, D.: & Cheng, P. Nonlinear Model Predictive Control of Floating Wind Turbines. ISOPE-I, https://10.1109/ACC.2014.6858718, June 2013.

Shan, M., Jacobsen, J., Adelt, S., Field Testing and Practical Aspects of Load Reducing Pitch Control Systems for a 5 MW Offshore Wind Turbine, European Wind Energy Conference and Exhibition, EWEC, https://doi.org/10.24406/publica-fhg-383237, 2013

Stockhouse, D., Phadnis, M., Grant, E., Johnson, K., Damiani, R. & Pao, L.: Control of a Floating Wind Turbine on a Novel Actuated Platform, https://doi.org/10.48550/arXiv.2110.14169, 2021.

510